



# Numerical Assessment of the Geothermal and Thermal Energy Storage Potential of the Underground Con Mine (Northwest Territories, Canada)

Dan David Ngoyo Mandemvo<sup>1</sup> · Félix-Antoine Comeau<sup>1</sup> · Jasmin Raymond<sup>1</sup> · Stephen E. Grasby<sup>2</sup> · Viktor Terlaký<sup>3</sup>

Received: 7 February 2023 / Accepted: 10 February 2024 / Published online: 4 April 2024  
© The Author(s) under exclusive licence to International Mine Water Association 2024

## Abstract

Flooded mines constitute groundwater reservoirs that can be exploited with geothermal heat pump systems. Modelling such a reservoir is challenging because groundwater flow and heat transport equations need to be solved within the complex geometry of mine workings. To address this challenge, we developed a tridimensional numerical model to estimate the geothermal heat pump and underground energy storage potential, using the Con Mine near Yellowknife, Northwest Territories, Canada as an example. We used the finite element method to simulate the transient 3D temperature field within the water and in the rock mass. The shafts and tunnels of the mine are represented with 1D elements embedded in a tridimensional matrix. Hydraulic and thermal properties were evaluated at the mine site and in the laboratory with samples from outcrops and cores. The numerical model was calibrated to reproduce hydraulic head and temperature measured while pumping one of the shafts. Then, the long-term temperature of the water under different cases of geothermal heat pump operation was simulated for 25 years. The total energy delivered to buildings per year for a flow rate of  $0.06 \text{ m}^3 \text{ s}^{-1}$  was 953 MWh vs. 18,048 MWh when the pump depth was 0.3 vs 1 km. We also simulated heat production using solar thermal collectors to provide additional energy storage. The results suggest that it would be easier to increase energy production by augmenting the flow rate or by placing the pump at a greater depth than by adding solar collectors.

**Keywords** Energy · Heat · Mine water · Heat pump · Finite element

## Abbreviations

### Symbols

$A$	[m <sup>2</sup> ] Area
$c$ [MJ m <sup>-3</sup> K <sup>-1</sup> ]	Volumetric heat capacity
$g$ [m <sup>2</sup> /s]	Gravitational acceleration
$h$ [m]	Hydraulic head
$K$ [m s <sup>-1</sup> ]	Hydraulic conductivity
$Q$ [W m <sup>-3</sup> ]	Heat exchange rate
$Q'$ [m <sup>3</sup> s <sup>-1</sup> ]	Water exchange or flow rate
$q$ [W m <sup>-2</sup> ]	Conductive heat flux
$SP$ [W]	Solar production
$STP$ [W m <sup>-2</sup> ]	Solar thermal production per area
$S$ [m <sup>-1</sup> ]	Specific storage
$s$ [Pa <sup>-1</sup> ]	Compressibility of the host rock
$T$ [K]	Temperature
$t$ [s]	Time
$u$ [m s <sup>-1</sup> ]	Velocity field

### Greek letters

$\beta$ [ $4.4 \times 10^{-10} \text{ Pa}^{-1}$ ]	Compressibility of water
$\epsilon$ [-]	Solar collector efficiency

✉ Jasmin Raymond  
jasmin.raymond@inrs.ca

Dan David Ngoyo Mandemvo  
dan\_david.ngoyo\_mandemvo@inrs.ca

Félix-Antoine Comeau  
felix-antoine.comeau@inrs.ca

Stephen E. Grasby  
steve.grasby@canada.ca

Viktor Terlaký  
viktor\_terlaký@gov.nt.ca

<sup>1</sup> Institut National de la Recherche Scientifique, Centre Eau Terre Environnement, 490 Rue de la Couronne, Québec City, QC G1K 9A9, Canada

<sup>2</sup> Geological Survey of Canada, 3303-33 Street NW, Calgary, AB T2L 2A9, Canada

<sup>3</sup> Northwest Territories Geological Survey, 4601-B 52nd Avenue, Yellowknife, Northwest Territories X1A 1K3, Canada

$\theta$ [-]	Porosity
$\lambda$ [ $\text{W m}^{-1} \text{K}^{-1}$ ]	Thermal conductivity
$\rho$ [ $\text{kg m}^{-3}$ ]	Density
<b>Indices</b>	
amb	Ambient
c	Injected in the mine water during cooling season
cooling	Cooling of the buildings
eff	Effective
g	Ground
h	Extracted from the mine water during heating season
heating	Heating of the buildings
<i>i</i>	Denoting the direction with subscripts <i>x</i> , <i>y</i> , and <i>z</i>
inj	Injection
prod	Production
r	Host rock
s	Solar thermal collector
w	Water
<b>Abbreviation</b>	
<i>COP</i>	Coefficient of performance

## Introduction

Mining creates karst-type aquifers through excavation of underground workings and the reopening of fractures in the rock mass surrounding the workings (Ordóñez et al. 2012). When mine dewatering ceases, at the end of mining activity, the connected voids are flooded and constitute a high-volume underground reservoir. A flooded mine comprises a network of shafts, tunnels, and drifts filled by water from three sources: precipitation, surrounding aquifers, and surface water bodies (including artificial lakes holding tailings). Infiltration of water into the mine depends on the natural permeability of the rock mass and the induced permeability linked to mine openings where water flows with little hydraulic resistance (Ghoreishi Madiseh et al. 2012). For this reason, abandoned mines with vast flooded tunnels can be advantageously used with geothermal heat pumps system to heat residential and commercial buildings (Renz et al. 2009). Geothermal energy is considered an ecologically friendly and economic alternative form of energy production in Canada (Grasby et al. 2012) and elsewhere. Geothermal heat pump installations have minor influence on the landscape in contrast to other “green” energy resources (water, wind, and solar). In addition, flooded mines typically have a large water storage capacity, and are thus suitable to manage the heat loads during peak-demand-periods (Ghoreishi Madiseh et al. 2012), acting as a thermal battery. The

advantages of mining environments are the storability of the Earth’s heat flow (Verdier-Gorcias 2016) and the significantly reduced capital cost compared to conventional closed and open loop systems that require extensive drilling (Roy et al. 2020).

Despite its potential, the use of mine water as a geothermal resource is uncommon (Lund and Toth 2021), although there are some active systems. In Canada, the use of geothermal energy from mine water started in the 1980s with the Springhill Nova Scotia project (Jessop et al. 1991), which pioneered geothermal heating based on the use of mine water. The Heerlen project in the Netherlands is one of the largest geothermal heating projects that use water from a flooded abandoned coal mine; it heats and cools 16,200 m<sup>2</sup> of community buildings, 350 dwellings, and 3,800 m<sup>2</sup> of commercial floor space (Hall et al. 2011). Four heat pumps with a capacity of 700 kW are actively providing 80% of the annual heat requirements.

More examples of successful small-scale implementations of mine water geothermal systems exist. In Germany, the Wismut Shaft 302 in Marienberg provides 690 kW of heating capacity to a sports complex and supermarkets (Matthes and Schreyer 2007) and in Freiburg, a mine gallery is used to heat and cool a castle (Kranz and Dillenardt 2010). A section of the abandoned mine provides water at a flow rate of 3 L/s and 10.2 °C. In Norway, the former Folidal copper, zinc, and sulfur mine has been producing water to heat the underground Wormshall Cavern since October 1998 (Banks et al. 2004). In Scotland, flooded mines are used for space heating of 16 houses in Shettleston (Gilbert 2021a) and 18 houses in Lumphinnans (Gilbert 2021b). In the USA, a municipal building in Park Hills, Missouri, is heated with mine water and nine heat pumps that have a total capacity of 112 kW, with a total of 750 m<sup>2</sup> of space heated (Caneta Research 1997).

Successful development of geothermal heating systems from flooded mines has prompted many studies assessing the feasibility of mine water systems in various locations worldwide (e.g. Jardón et al. 2013; Wieber and Pohl 2008). A study in Hungary showed that an abandoned copper mine possesses a resource of 2.88 MW that could be used for district heating, or heating spas and swimming pools at a nearby wellness centre (Toth 2007). A system like that of the Follidal mine in Norway was designed to use the mine water energy from the shaft to heat a mining museum, as well as a banquet and concert hall located 342 m below the surface (Banks et al. 2004). In Poland, the closed and abandoned Nowa Rudat mine possesses an estimated water volume of 5,000,000 m<sup>3</sup> and the available power was quantified between 0.8 and 1.6 MW (Małolepszy 2003). The Midlothian coal mine in Scotland could be capable of space heating for dwellings covering 15,000 m<sup>2</sup> and a 12,000 m<sup>2</sup> school, with a total of 3 MW extractable energy (Hall et al.

2011). In the USA, a feasibility study of an abandoned coal mine in Pittsburgh showed that the energy contained in that mine could reach 437 GWh and could be used for space heating (Watzlaf and Ackman 2006).

Several feasibility studies were also performed in Canada. In Timmins, Ontario, the abandoned MacIntyre and Hollinger gold mines were studied. The heat from these two mines could be used for space heating of a hospital and a local arena, but the project appeared to be uneconomical. Space heating of the Shania Twain Center (museum) was suggested as an alternative option (Hall et al. 2011). The potential of the Gaspé Mines in Québec was evaluated by Raymond and Therrien (2014), indicating a minimum annual energy availability of 1.48 GWh for space heating using a flow rate of  $0.019 \text{ m}^3 \text{ s}^{-1}$ , and  $\approx 4.5$  GWh if the flow rate was increased to  $0.063 \text{ m}^3 \text{ s}^{-1}$ .

Numerical models are useful for evaluating the geothermal potential of a mine site (Purba et al. 2021), but it can be difficult to represent the complex geometry of the mine workings, given the vertical and lateral interconnectivities and the heterogeneity of the surrounding rock. Additionally, the lack of subsurface data makes numerical modelling difficult. Numerical models use approximation to solve flow and heat transport equations (Loredo et al. 2016). Modelling a flooded mine for geothermal energy recovery is thus a great challenge, because of the multiphysical phenomena involved. Numerical models require the initial development of a conceptual model to simulate heat transfer mechanisms with appropriate solutions, and different hypotheses can be tried to replicate field observations. Once a model satisfactorily reproduces observations, it can be used for predictions (Brown and Trott 2014). Different modelling strategies are available including 2D and 3D representation of the mine system. In these models, it can be easier to represent elongated features such as shafts and tunnels by 1D elements. For instance, Renz et al. (2009) developed a 2D Darcy flow model with the finite element simulator FEFLOW for the Stassfurt potassium mine in Germany. Laminar flow was assumed in the roadways and the shafts were represented by 1D elements.

Another way to approach the modelling problem is to use an integrated finite difference method for space discretization. For example, the heat exchange process at the flooded workings of the Nowa Ruda mine in Poland was evaluated by Małolepszy (2003) with TOUGH2 in such a 2D model. The geothermal potential of some abandoned mines in China was also evaluated with a 3D model in TOUGH2 by Guo et al. (2018).

The finite volume approach was employed by Hamm and Bazargan Sabet (2010). They used the MARTHE simulator to assess the thermal depletion due to cold water reinjection in the Lorraine coal mine in France. Two hydraulic schemes were compared, with production/injection in different shafts

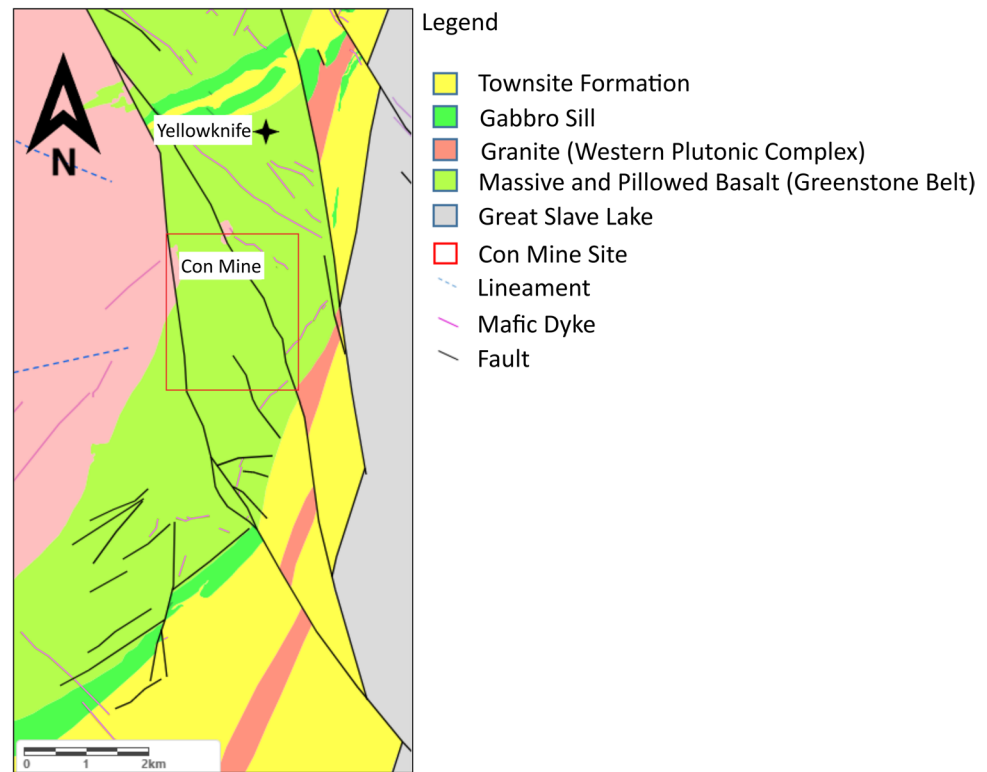
and in the same shaft. The simulations showed that at the extraction point, the temperature decreases and tends to stabilize with time. Bao and Liu (2019) also used a finite element volume method implemented with C++ to simulate a double diffusive flow based on temperature and salinity differences. Their numerical analysis described the transient heat extraction from a flooded mine shaft affected by thermohaline stratification and showed that heat extraction doesn't markedly affect the thermohaline stratification for a flow rate of  $0.00014$  to  $0.03 \text{ m}^3 \text{ s}^{-1}$  whereas it does have an impact for a flow rate hundred times higher.

Over the past century, the underground gold mines (Giant and Con) developed in Yellowknife, Northwest Territories, Canada have changed the natural groundwater flow patterns in the area. There are now underground anthropogenic voids caused by mining activity and secondary porosity generated by mining-induced fracturing. Seasonal pumping and treatment of mine water is performed at those sites to avoid any contamination of surrounding surface and groundwater. According to Wolkersdorfer (2006), these systems can be called "mine aquifers". Preliminary geothermal potential studies on the Con Mine by Ghomshei (2007) provided a conceptual model to determine the feasibility of using the mine water for geothermal heating of a residential apartment building in downtown Yellowknife and determined a maximum payback period of eight years for the capital investment. Ghomshei (2007) used the volumetric method of Muffler and Cataldi (1978) to determine the geothermal potential of the mine based on the knowledge of the mine volume, the volumetric heat capacity of water, and the temperature difference before and after heat extraction. Only the energy contained in the volume of water flooding the mine was considered to estimate the geothermal potential. The Con Mine heat resource was also evaluated by Ferket et al. (2012) to have a capacity of 0.4 MW, based only on the natural heat flow.

Both previous studies likely underestimated the geothermal potential of the Con Mine. Recent work by Ngoyo Mandemvo et al. (2023) for the Con Mine suggested a geothermal potential of 2 MW, considering the thermal mass of water inside and infiltrating the mine as well as the surrounding host rock. However, convective heat transfer was neglected with this preliminary analytical approach that was developed to provide a first estimate of geothermal resources. Further studies were thus needed to carefully evaluate the mine's geothermal potential. We believe temperature profiles as well as field and laboratory analysis of hydraulic and thermal properties can reduce the uncertainty of the mine's geothermal potential.

Thus, the objective of this work was to develop a comprehensive numerical model that includes groundwater flow and heat transfer to simulate the geothermal system operation and to fully assess the geothermal potential of

**Fig. 1** Detailed geological map in the vicinity of the Con Mine site (modified from Northwest Territories Geological Survey 2021)



the Con Mine site, opting for a model that considers the complex geometry of the mine. We can simulate natural phenomena with such a numerical approach, considering the convective heat transfer in the rock mass and underground workings under the local geothermal gradient. The goal was to simulate pumping and reinjection of groundwater in the mine shafts to calculate the thermal output and the area of buildings that can be heated with a geothermal heat pump system operated with the mine water. The flow rate and depth of the pump were considered variable according to the heat demand of the buildings. To numerically solve the multiphysical processes involved in the mine system, a fully coupled tridimensional model based on the finite element method was developed for the Con Mine. Mining tunnels were represented by 1D elements while stopes and the surrounding rock were 3D. The model was calibrated to reproduce the temperature and hydraulic head measured during pumping in the mine shaft. The results allowed us to determine the energy available from the mine and estimate the number of different buildings that could be heated with mine water.

In this work, we also coupled the heat extraction from the mine with heat production from solar thermal collectors considered as input to underground energy storage, using guidelines of Sarbu and Sebarchievici (2017), to determine if surplus energy can be sent underground for storage after the heat from solar thermal collectors is directly used by buildings. Such underground energy

storage is not commonly considered for the geothermal potential assessment of mine water.

## Study Area

The Con Mine is located in the Northwest Territories, near the city of Yellowknife, Canada. Mining activities extended from 1938 to 2003. The average annual atmospheric temperature is  $-4.6$  °C. Annual precipitation in the Con Mine area based on a six-year average is 366.5 mm, with 164.7 mm of snow and 201.8 mm of rain. Average annual evaporation is 48 mm (Miramar Con Mine Ltd 2007). The Con Mine was developed in the Yellowknife Greenstone Belt of the Slave Geological Province (Miramar Con Mine Ltd 2007). The Greenstone Belt (Fig. 1) is bounded to the west by younger granitic rocks of the Western Plutonic Complex (Cairns and Hauser 1995). The Greenstone Belt consists of a succession of mafic to intermediate volcanic rocks (massive and pillow basalts) with small inclusions of volcanoclastic and sedimentary rocks to the northeast (Miramar Con Mine Ltd 2007). Many of the pillows are globular lava sacs with thick selvages and elongate branching patterns. Near the top of the mine, there are coarse sandstones and conglomerates interbedded with pillowed and massive basalts (Padgham 1980). Gold mineralization in the Yellowknife area, including the Con Mine property, is linked to south-striking and west-dipping shear zones. The shears hosting gold mineralization are the Con and Campbell Shear zones formed during

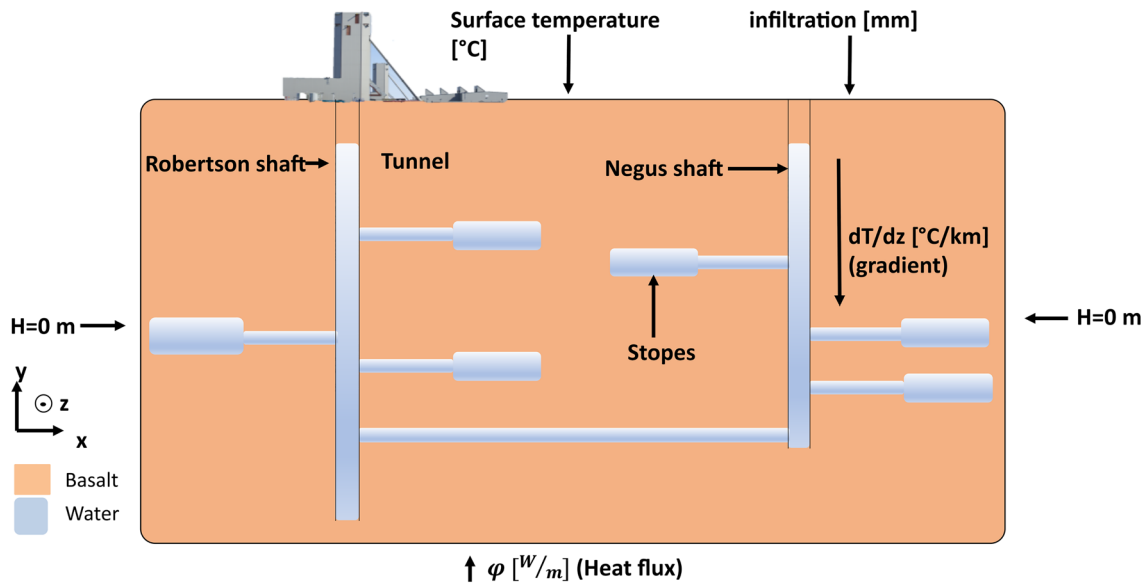


**Fig. 2** Conceptual model of the underground mine in 2D with initial and boundary conditions. Drawing not to scale. The distance between the Robertson and Negus shafts is about 430 m. Water was hypoth-

esized to be pumped in the Robertson shaft at a depth of 300 m or 1 km and injected in the Negus shaft for geothermal system operation

the intrusion of the granodiorite batholith of the Western Plutonic Complex mineralization (Miramar Con Mine Ltd 2007). The shear zones are predominantly composed of chlorite-carbonate schist with increasing sericite, sulphide, and quartz content in the areas of higher gold mineralization (Miramar Con Mine Ltd 2007).

## Methods

The assessment of the geothermal potential of the Con Mine was done in three steps. The first was to develop a numerical model that could be used to simulate geothermal heat pump system operations with pumping and injection of groundwater in the mine. Conductive and advective heat transfer was simulated with flow in the rock mass described by Darcy's Law. Shafts, mine tunnels, and stopes were represented in the model. Water flows through the mine tunnels with a uniform flow based on position and time. The COMSOL Multiphysics program (Comsol AB 2017) was used to develop the model relying on the finite element method to solve the flow and heat transfer equations. The second step consisted of calibrating the model using dewatering data provided by Newmont Mining Corp. Predictive simulations could be achieved with a calibrated model in the third step to evaluate the energy that could be extracted and injected from the mine and delivered with heat pumps to evaluate the number of buildings that can be heated and cooled from the mine's water. Different pumping depths and flow rates were simulated along with energy storage scenarios to evaluate

geothermal potential of the site. Energy storage scenarios were assumed to rely on solar thermal collectors installed at the mine site. The idea was to determine how many solar thermal collectors would be required to add one unit of archetype buildings and to evaluate whether solar thermal collectors would increase the net heating capacity.

Adaptative time steps with a maximum of 1 day for the calibration simulations and 1 month for the predictive simulations were used. The time required to run the predictive simulations was about 0.5 h on a desktop computer equipped with a 2.10 gigahertz dual core processor and 144 gigabytes of random access memory.

## Numerical Model

The model considers two distinct media (Fig. 2): the water and the host rock. The operation of a geothermal doublet was simulated with coupled subsurface flow and heat transfer. The host rock was assumed to be dominantly basalt according to the local geology. The mine tunnels are represented by linear 1D elements, and the stopes and host rock by 3D elements (Fig. 3). Mine tunnels were represented by 1D elements to reduce the number of elements and the computing time. The simulated flow field was composed of velocity vectors for water along and inside the tunnels and stopes. Subsurface flow was described by Darcy's Law and solved in 3D porous media and was also used to represent flow in the 1D tunnels. This approach assumes a laminar flow even in mine tunnels, which can underestimate heat exchanges associated to turbulent flow

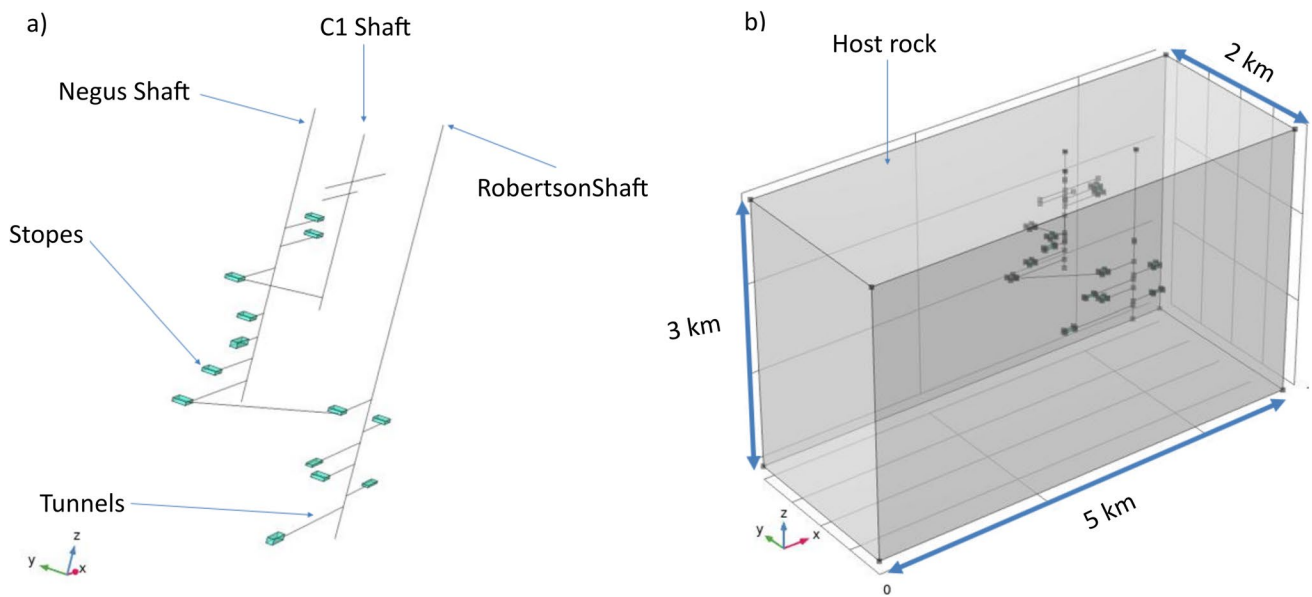


**Fig. 3** **a** Geometry of the mine workings, and **b** geometry of the model showing the host rock domain. Tunnels are represented in the numerical model by 1D elements while stopes and host rock by 3D elements

of a specific tunnel section. Simulating turbulent flow in voids is computationally intensive and the assumption of laminar Darcy flow was considered reasonable by Renz et al. (2009) who compared various turbulent vs. non-turbulent modeling approaches. Such simplifications are required when simulating flow and heat transfer in an underground mine system but should have a reasonably small impact on the global temperature response of the system if the hydraulic conductivity assumed for voids can be properly calibrated. Thus, fluid flow in the host rock and stopes is represented by Eq. (1), in the tunnels by Eq. (2), and specific storage by Eq. (3) (Comsol 2017):

$$S \frac{\partial h}{\partial t} = \frac{\partial}{\partial x} \left( K_x \frac{\partial h}{\partial x} \right) + \frac{\partial}{\partial y} \left( K_y \frac{\partial h}{\partial y} \right) + \frac{\partial}{\partial z} \left( K_z \frac{\partial h}{\partial z} \right) \pm Q' \quad (1)$$

$$S \frac{\partial h}{\partial t} = \frac{\partial}{\partial i} \left( K_i \frac{\partial h}{\partial i} \right) \quad (2)$$

$$S = \rho_w g (s + \theta \beta) \quad (3)$$

where  $K_i$  [ $\text{m s}^{-1}$ ] is the hydraulic conductivity (where  $i$  denotes the axial direction of the tunnels), and  $h$  [m] is the hydraulic head,  $S$  [ $\text{m}^{-1}$ ] is the specific storage,  $\rho_w$  [ $\text{kg m}^{-3}$ ] is the density of water,  $\beta$  [ $4.4 \times 10^{-10} \text{ Pa}^{-1}$ ] is the compressibility of water,  $\theta$  [-] is the porosity,  $s$  is the compressibility of the host rock [ $1.92 \times 10^{-14} \text{ Pa}^{-1}$ ], and  $Q'$  [ $\text{m}^3 \text{ s}^{-1}$ ] represents the effect of sources and sinks on the porous medium.

The heat transfer equations to be solved numerically are for the host rock and stopes (4) and for the shafts and mining tunnels (7). Equation (5) represents the volumetric heat

capacity while Eq. (6) and (8) represent the conductive heat flux (Freeze and Cherry 1979):

$$Q = (\rho c)_{\text{eff}} \frac{\partial T}{\partial t} + \rho c \mathbf{u} \nabla T + \nabla \mathbf{q} \quad (4)$$

$$(\rho c)_{\text{eff}} = \rho_w c_w \theta + (1 - \theta) \rho_r c_r \quad (5)$$

$$\mathbf{q} = -\lambda_r \nabla T \quad (6)$$

$$Q = (\rho c)_{\text{eff}} \frac{\partial T}{\partial t} + \rho c \mathbf{u} \frac{\partial T}{\partial i} + \nabla \mathbf{q} \quad (7)$$

$$\mathbf{q} = -\lambda_r \frac{\partial T}{\partial i} \quad (8)$$

where  $T$  [K] is the temperature,  $\mathbf{u}$  is the velocity field computed by the Darcy's Law,  $Q$  [ $\text{W m}^{-3}$ ] is the total heat transfer rate per unit volume,  $\rho_r$  [ $\text{kg m}^{-3}$ ] is the density of the host rock,  $c_r$  [ $\text{W m}^{-1} \text{ K}^{-1}$ ] is the volumetric heat capacity of the host rock,  $c_w$  [ $\text{W m}^{-1} \text{ K}^{-1}$ ] is the volumetric heat capacity of water,  $\mathbf{q}$  [ $\text{W m}^{-2}$ ] is the conductive heat flux, and  $\lambda_r$  [ $\text{W m}^{-1} \text{ K}^{-1}$ ] is the thermal conductivity.

The model domain has a length of 5 km in the  $x$  direction, a width of 2 km in the  $y$  direction, and a depth of 3 km in the  $z$  direction. Simulations conducted with different thermal loads verified that the chosen domain was sufficiently large such that the thermal plume produced by the production and reinjection activities would not interfere with the lateral boundaries of the model. The domains of the model are made of mine tunnels, stopes, and the surrounding host

**Table 1** Properties of the numerical model units

Properties	Host rock		Stopes		Tunnels	
	Min	Max	Min	Max	Min	Max
Porosity [-]	0.008	0.25	0.1	0.5	1	1
Permeability [cm <sup>2</sup> ]	$9.8 \cdot 10^{-11}$	$9.8 \cdot 10^{-10}$	$10^{-9}$	$10^{-6}$	$10^{-5}$	$10^{-2}$
Hydraulic conductivity [m s <sup>-1</sup> ]	$9.6 \cdot 10^{-8}$	$9.6 \cdot 10^{-7}$	$9.8^{-7}$	$9.8^{-4}$	$9.8^{-3}$	9.8
Storage coefficient [m <sup>-1</sup> ]	$3.5 \cdot 10^{-8}$	$1.1 \cdot 10^{-6}$	$4.3 \cdot 10^{-7}$	$2.2 \cdot 10^{-6}$	$4.3 \cdot 10^{-6}$	$4.3 \cdot 10^{-6}$
Density [kg m <sup>-3</sup> ]	3,016		3,016		1,000	
Heat capacity [J kg <sup>-1</sup> K <sup>-1</sup> ]	725		725		4,185	
Thermal conductivity [W m <sup>-1</sup> K <sup>-1</sup> ]	3.5		3.5		0.6	

**Table 2** Grid sizes chosen for the independence study

Grid	Minimum grid size	Maximum grid size	Number of elements
1	90	500	12,988
2	50	400	21,185
3	20	275	53,16
4	7.5	175	162,398
5	1	100	590,159
6	1	95	674,542
7	1	85	908,983

rock. The properties associated with the host rock, stopes, and mine tunnels are shown in Table 1. Vertical shafts are assumed to have the same properties as tunnels although stopes have different properties than tunnels because stopes can be backfilled. Host rock properties were measured in the laboratory with rock samples from the mine or assessed in the field (Ngoyo Mandemvo 2022). Twenty-five unaltered basaltic samples were obtained from cores and outcrops with a maximum radius of 1.5 km surrounding the principal mine shaft. A thermal conductivity scanner was used to evaluate thermal conductivity and heat capacity in the laboratory. Porosity and density of the rock matrix were determined with a gas porosimeter in the laboratory. Hydraulic conductivity and permeability of the fractured rocks were evaluated with structural geology surveys conducted around the mine using the scanline method and the cubic law (Ngoyo Mandemvo 2022). 1430 fracture measurements were taken at nine outcrop locations within a 2 km radius surrounding the mine principal shaft. Fracture spacing allowed calculation of a range of hydraulic conductivity values depending on the potential fracture opening at depth. An equivalent porous media approach was used with the model to assign hydraulic properties and simulate flow in the rock surrounding the mine. Major faults were not considered in the model because the state of stress is unknown and it would be difficult to determine whether the faults could behave as hydraulic barriers or pathways. Groundwater flow in the models was also assumed to dominantly respond from the hydraulic property contrast between the host rock and the mine excavations.

The model also assumes that natural convection inside the rock mass is negligible compared to the forced convection due to the water pumped inside the mine tunnels. Figure 2 shows a schematic drawing of the model geometry. One shaft (Robertson) is assumed to be used for water production and another shaft (Negus) for injection.

The flow boundary conditions include a specified flux at the top to represent recharge from precipitation for the city of Yellowknife, evaluated at 72.5 mm/year (Miramar Con Mine Ltd 2007). At the model lateral boundary (Fig. 3), the hydraulic head was fixed to zero, representing the water level

in the surrounding lakes. At the bottom of the model, there was no flow. The initial condition was a uniform hydraulic head equal to zero as the regional hydraulic gradient in the flat topographic setting of the Con Mine is expected to have little influence on flow compared to the drawdown triggered by pumping.

The temperature at the top of the model was 0.14 °C and was determined using the relationship of Ouzzane et al. (2015):

$$T_g = 17.898 + 0.951T_{amb} \tag{9}$$

where  $T_g$  [K] is the undisturbed ground temperature and  $T_{amb}$  [K] is the mean atmospheric temperature at the surface. A heat flux of 59.13 mW m<sup>-2</sup> was used based on the local geothermal gradient (Jessop 2005; Ngoyo Mandemvo 2022) and was assigned at the bottom of the model, such that temperature increased with the geothermal gradient and reproduced measurements made in Yellowknife (17.4 °C km<sup>-1</sup>; Ngoyo Mandemvo 2022).

### Meshing and Time Step

The model mesh is tetrahedral. The mesh independence was evaluated to obtain the best grid size for the simulations. We tested seven different grid sizes (Table 2) to find out their effect on the production temperature while pumping at 0.01 m<sup>3</sup> s<sup>-1</sup> (average flow rate of dewatering in the C-1 shaft) for 25 years, which corresponds to the lifetime of a geothermal heat pump system. The results show that there was no significant change in temperature beyond the grid size, ranging from 1 to 100 m. The grid size is the length of each side of the cells (Fig. 4).

The calibration and predictive simulations modeled a period of nine months of water pumping and rebound and 25 years of geothermal heat pump system operation,

respectively. An adaptable time step scheme was used for both cases where the solver automatically chose the length of the time steps to ensure convergence within a maximum time step allowed. The maximum time steps for the calibration and predictive simulations were 1 day and 1 month, respectively. We used a maximum monthly time step for predictive simulations because the heat demand (input) data was given for every month of the year. However, the computed time steps were commonly less than a month to ensure convergence was reached. Thus, a total of 300 months were simulated to evaluate temperature fluctuations between heating and cooling seasons.

### Calibration and Sensitivity Analysis

Model calibration was made to reproduce the field observations with the numerical model. The optimum parameters can be set by manual calibration or with algorithms (Sunmin 2021). In our case, the calibration of the model was to reproduce the observed water level and temperature during dewatering activities of the Con Mine. During the summer, pumping was started to avoid flooding and to keep the water level at about 70 m below the surface. At the end of summer, the pumping is shut down until the next year. With the hydraulic head and temperature calibrated, we could predict the drawdown and the mine water temperature during the pumping operations. The available water level and temperature data were for the period of June 2019 to March 2020. The permeability and porosity of the host rock, tunnels, and stopes were adjusted manually to fit the observed water level and temperature.

Preliminary simulations during calibration suggested that permeability and porosity of the host rock have the greatest influence on the system’s response. A sensitivity analysis was performed to evaluate the influence of the permeability and porosity on the water-level and temperature by varying

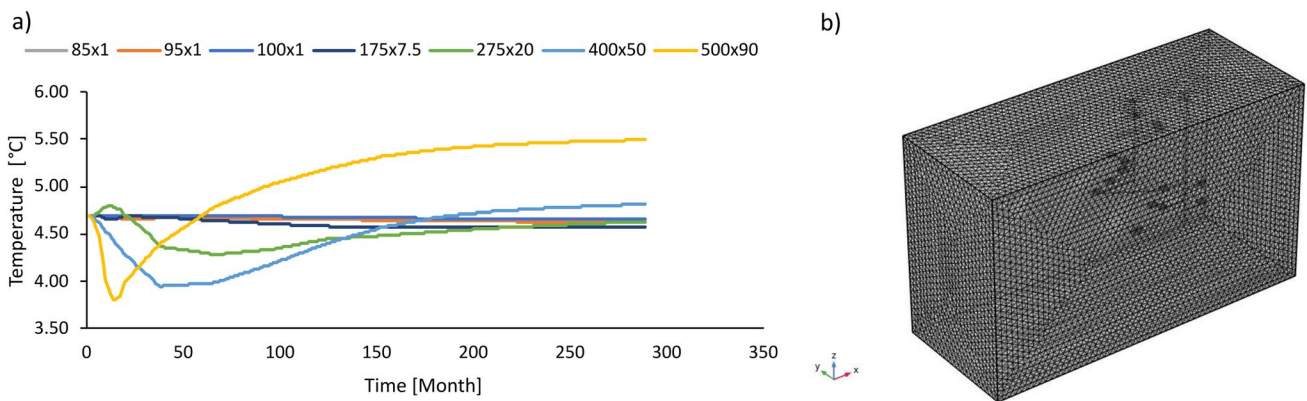


**Fig. 4** a Influence of grid sizes on pumped water temperature for the mesh independence study, and b model with the grid size chosen for the simulations. The chosen minimum mesh size is 1 m and the maximum mesh size is 100 m for a total of 590,159 elements



the value of the permeability and porosity of the host rock one at a time.

### Determination of the Space Load with EnergyPlus

A database of the American Society of Heating, Refrigerating and Air Conditioning Engineers provides data on surface and space load of archetype buildings located in Denver, USA. The simulation files of archetype buildings (EnergyPlus 2021) were used to simulate the heating and cooling needs of different buildings in Yellowknife by changing the weather data file within the EnergyPlus software considering climate normals from the past 30 years (Environment and Climate Change Canada 2021).

### Energy Storage

Sunlight energy can be captured by solar thermal collectors and transformed into heat for heating buildings and potential storage in mine water. The power output from a solar thermal collector depends on its size and efficiency. The heat collected is evaluated by multiplying the solar production of a collector by the average hours of sunlight in a month. Solar thermal collectors production ranges from 250 to 400 W per unit (Energysage 2021). Our model uses a typical solar thermal collector of 290 W that has a surface area of 1.6 m<sup>2</sup> (Energysage 2021). We evaluated the amount of heat produced by solar thermal collectors based on average hours of sunlight in Yellowknife, again using 30 years climate normals from Environment and Climate Change Canada (2021). Knowing the amount of heat collected, the effective solar production per month was calculated by accounting for the solar collector efficiency, which can range from 8 to 44% (Krawczyk et al. 2020), and by using reflectors the efficiency can reach 61% (Bhowmik and Amin 2017). For a solar thermal collector of 290 W, an average efficiency of 20% is appropriate (Energysage 2021; Yellowlite 2021). Thus, the following relationship was used to assess the solar production (Krawczyk et al. 2020):

$$SP = STP \times A_s \times \epsilon \quad (10)$$

where  $SP$  [W] is the total solar production,  $STP$  [W m<sup>-2</sup>] is the solar thermal production per area,  $A_s$  [m<sup>2</sup>] is the solar thermal collector area, and  $\epsilon$  [-] is the solar collector efficiency, which was assumed to vary on a monthly basis in our study. The heat produced by the solar thermal collector was assumed to be directly used in buildings. Surplus heat production, for example in summer months, was then injected into the mine water. When solar did not produce enough energy to sufficiently heat all of the buildings, the geothermal heat pump system was assumed to deliver the remaining heat.

### Prediction of Geothermal Operations

The maximum power that could be extracted from the mine water depended on the pumping rate and the injection temperature. To allow continuous production, the water injected in the shaft must not be less than 2 °C to avoid freezing. Increasing the pumping rate increases the drawdown in the pumping shaft, but the hydraulic head must not be lower than the pump elevation; otherwise, it won't be possible to pump water from the mine. To estimate the injection temperature during the predictive simulations aiming to reproduce geothermal operations, we used the following equations describing heat exchange at the heat pump (Cengel and Boles 2006):

$$T_{inj} = T_{prod} + \frac{Q_h}{C_w \times Q'} + \frac{Q_c}{C_w \times Q'} \quad (11)$$

$$Q_h = Q_{heating} \times \frac{(COP_{heating} - 1)}{COP_{heating}} \quad (12)$$

$$Q_c = Q_{cooling} \times \frac{(COP_{cooling} + 1)}{COP_{cooling}} \quad (13)$$

where  $T_{inj}$  [°C] is the injection temperature,  $T_{prod}$  [°C] is the production temperature at the pumping depth,  $Q'$  [m<sup>3</sup> s<sup>-1</sup>] is the water flow rate, and  $COP$  [-] is the heat pump coefficient of performance. For the calculation, the  $COP$  is assumed constant through time,  $Q_{heating}$  and  $Q_{cooling}$  [W] are the space load of the buildings (negative in heating and positive in cooling), and  $Q_h$  and  $Q_c$  [W] are the power extracted or injected from the mine water (negative in heating and positive in cooling). The number of buildings was gradually increased in the simulation to increase the building loads until the injection temperature was below 2 °C, which allowed the geothermal potential to be evaluated at a given flow rate.

## Results

### Calibration Simulations

The regular mine-dewatering operations occur only during the summer to avoid over flooding. Therefore, the numerical model was calibrated according to the temperature and the flow rate measured at the C-1 shaft during one annual dewatering operation. The quality of the fit was evaluated with the Pearson correlation coefficient  $R^2$ . This coefficient quantifies the strength of the relationship between the simulated and the measured water level and temperature. A coefficient value close to one means a good correlation between the two

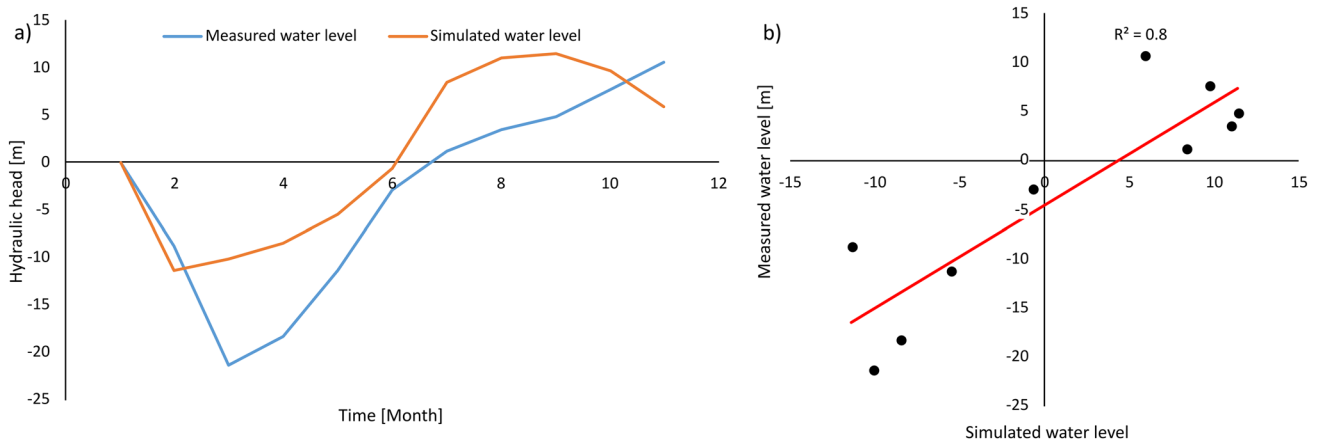


**Fig. 5** **a** Hydraulic head measured and simulated during mine water dewatering that took place in the C-1 shaft from July to September 2019 and the natural elevation of the water level recovering during September to March 2020. **b** Calculation of correlation coefficient

between measured versus simulated hydraulic head recorded during mine water dewatering that took place in the C-1 shaft from July to September 2019 and the natural elevation of the water-level recovery during September

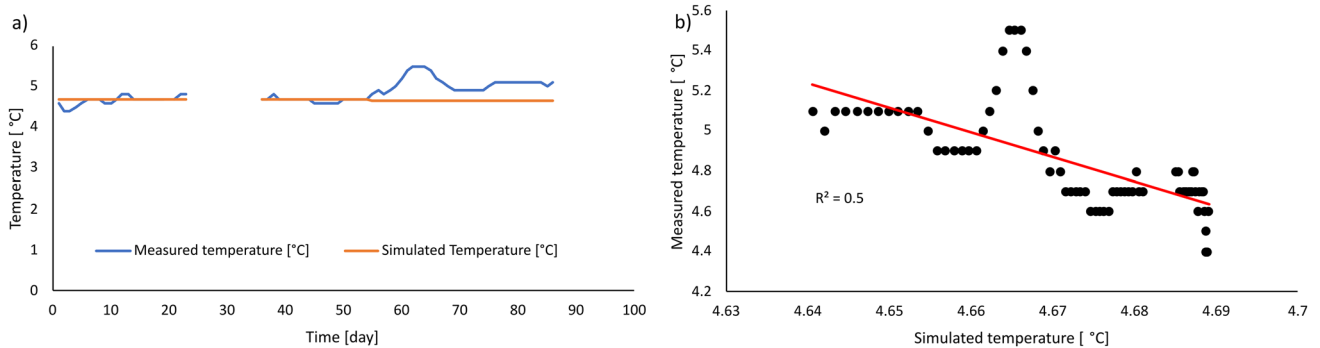


**Fig. 6** **a** Simulated and measured temperature during mine water dewatering that took place in the C-1 shaft from July to September 2019. **b** Calculation of correlation coefficient between measured ver-

sus simulated temperature recorded during mine water dewatering that took place in the C-1 shaft from July to September 2019

variables. The numerical model was able to reproduce the trend in hydraulic head, although the exact head values were not fully reproduced (Fig. 5a). The first three months of simulations were for the pumping period (at an average flow rate of  $0.01 \text{ m}^3 \text{ s}^{-1}$ ) when the hydraulic head decreased. Pumping was stopped in the following months when the water level rose. Simulated hydraulic heads fit observed hydraulic heads with a correlation coefficient of 0.8, but overestimated heads by an average of 4.5 m throughout most of the dewatering period (Fig. 5b). For a complex system like a mine, this gap was acceptable. A delay can be seen for the maximum and minimum hydraulic head when comparing measured and simulated values. Hydraulic head is highly dependent on the flow rate, which was manually measured by the mine staff and for which there could be errors. Knowing this uncertainty, our goal was to reproduce the measured hydraulic head tendency, but not the exact values.

The simulated temperature closely approximated the observed temperature during the first 20 days of pumping. For the last 30 days, however, the measured temperature seemed perturbed (Fig. 6a). Water exiting the dewatering outlet zone was exposed to atmospheric conditions and to mixed water coming from various depths, which created temperature fluctuations that could not be replicated exactly (Fig. 6a). The correlation coefficient was 0.5 (Fig. 6b).

**Sensitivity**

Different values of permeability and porosity of all model units were used to calibrate the model. Calibration runs show that hydraulic head was predominantly affected by permeability changes, and temperature was most sensitive to porosity changes. The sensitivity of the parameters from tunnels and stopes were relatively weak compared to the host rock. The parameters of the host rock had the greatest

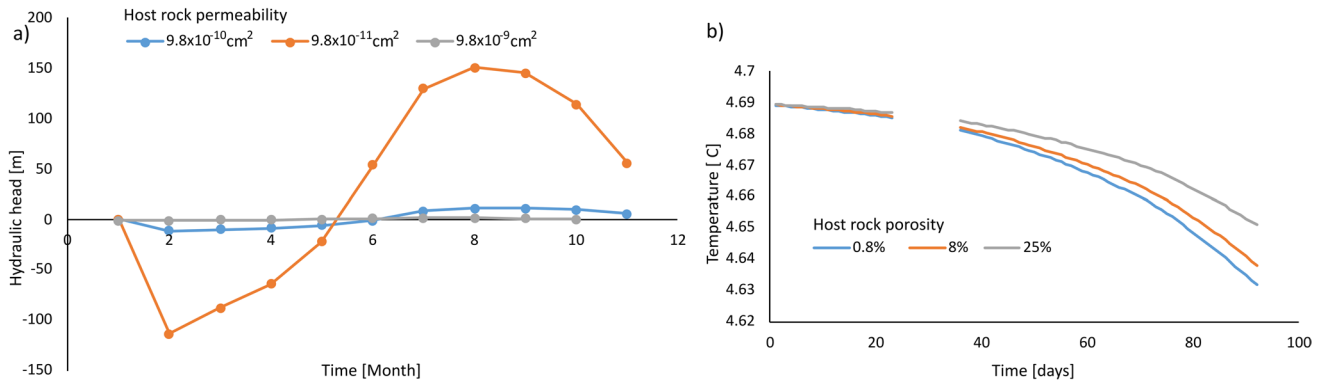


**Fig. 7** a Simulated hydraulic head during mine water dewatering that took place in the C-1 shaft from July to September under different host rock permeability. b Simulated temperature during mine water

dewatering that took place in the C-1 shaft from July to September under different host rock porosities. Between 20 and 40 days, no temperature data was recorded by the mining staff

**Table 3** Building monthly loads (MWh) and peak loads (kW) determined according to Yellowknife weather conditions. Negative is for heating and positive for cooling

	Mid-rise apartment		Fast food		Retail stand-alone		Medium office		Small hotel		Outpatient healthcare	
	MWh	kW	MWh	kW	MWh	kW	MWh	kW	MWh	kW	MWh	kW
January	-78	-104	-63	-85	-107	-144	-181	-243	-153	-206	-209	-281
February	-64	-95	-60	-83	-90	-133	-158	-235	-137	-203	-182	-271
March	-40	-54	-53	-72	-76	-102	-153	-206	-135	-182	-191	-256
April	-18	-26	-37	-52	-39	-54	-76	-106	-106	-148	-125	-174
May	-5	-7	-26	-36	-15	-20	-28	-37	-90	-121	-71	-95
June	5.8	8.0	0.05	1.7	2.5	3.5	10.8	14.5	18.7	25.1	39.5	54.8
July	5.8	7.7	0.05	1.7	2.5	3.4	10.1	14.0	17.5	24.3	39.5	53.1
August	5.8	7.7	0.05	1.7	2.5	3.4	10.1	14.0	17.5	24.3	39.5	53.1
September	5.8	8.0	0.05	1.7	2.5	3.5	10.8	14.5	18.7	25.1	39.5	54.8
October	-26	-35	-34	-46	-32	-44	-62	-84	-97	-131	-107	-144
November	-56	-78	-48	-66	-63	-87	-120	-166	-121	-168	-164	-227
December	-74	-99	-61	-83	-93	-125	-176	-236	-149	-200	-208	-280
Heating	-361		-384		-514		-953		-989		-1,256	
Cooling	23		0.21		10		42		72		158	

influence on the calibration of the hydraulic head and temperature. A host rock permeability of  $9.8 \times 10^{-10} \text{ cm}^2$ , tunnel permeability of  $10^{-4} \text{ cm}^2$ , and stope permeability of  $10^{-6} \text{ cm}^2$  resulted in the best model fit; other values tended to over- or under-estimate the observed hydraulic head (Fig. 7a). The porosity of the host rock that gave the best match for the observed temperature was 0.8% (Fig. 7b), which corresponds to that measured in the laboratory for the host rock matrix (Ngoyo Mandemvo 2022). A porosity of 100% and 25% was assumed for the empty tunnels and backfilled stopes, respectively.

### Building Energy Analysis

The energy extracted and injected to the mine water depends on the heating and cooling demand of each archetype building. The buildings selected for the sake of the simulation were those available in the EnergyPlus database: fast food, retail stand-alone, outpatient healthcare, small hotel, medium office, and mid-rise apartment. The needs of different buildings depend on their size. The required heating energy peaks are in January and December. The small hotel has the second-highest energy demand and also the greatest peak load (Table 3).

The power and energy produced by solar thermal collectors were assessed seasonally according to the characteristics chosen for the solar thermal collector (rated production of

**Table 4** Sunlight hours, panel power and total energy produced per month per solar thermal collector covering an area of 1.6 m<sup>2</sup>

	Sunlight h	Panel power W	Total energy Wh
January	50.6	14.7	743
February	107.3	31.1	339
March	188.4	54.6	10,293
April	276.4	80.1	22,155
May	335.7	97.4	32,681
June	373.8	108.0	40,521
July	358.0	103.0	37,167
August	276.2	80.1	22,123
September	157.7	45.7	7,212
October	65.0	18.9	1,225
November	42.7	12.3	529
December	24.6	7.1	175

290 kW for a 1.6 m<sup>2</sup> area; Energy Sage 2021). Table 4 presents the sunlight hours (Environment and Climate Change Canada 2021), the monthly panel power, and the total energy produced per month by a solar thermal collector.

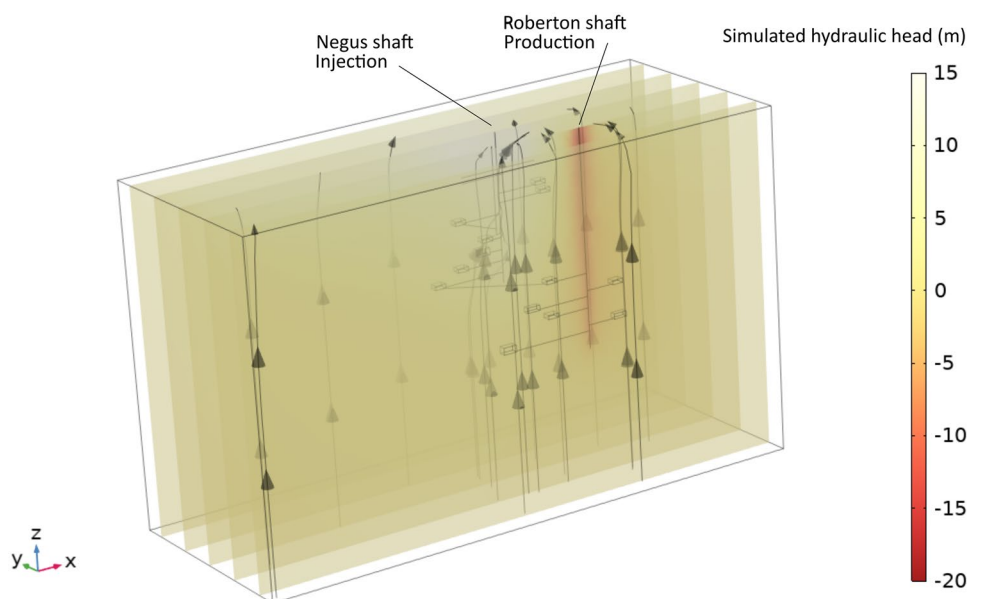
### Predictive Simulations of Geothermal System Operation

Two flow rates were used to pump water out of the mine. These flow rates must not be too high to avoid drawdown below the pump depth and to prevent natural flooding of the shaft used for water injection. Water level simulations indicate that pumping rates between 0.06 m<sup>3</sup> s<sup>-1</sup> and 0.08 m<sup>3</sup> s<sup>-1</sup>

do not present a risk of excessive drawdown or flooding. Drawdown and buildup at the pumping and injection wells for the case where the geothermal system is operated at a flow rate of 0.06 m<sup>3</sup> s<sup>-1</sup> is shown on Fig. 8, with streamlines indicating the heat flux direction. The heat flux is mostly vertical due to the natural geothermal gradient but slightly diverted near the pumping and injection wells. Additionally, mine dewatering is taking place each summer in the C-1 shaft to make sure the mine water level remains below that of the surrounding lakes. Simulations of geothermal heat pump system operations were made to compare cases with and without pumping water each summer in the C-1 shaft at a flow rate of 0.01 m<sup>3</sup> s<sup>-1</sup> to include mine dewatering activities. The aim was to verify if the summer dewatering influenced the water level already affected by pumping in the Robertson shaft and injection in the Negus shaft. The Robertson shaft was selected as the pumping shaft because the water is warmer in this deeper shaft. The water level appears not to be influenced by summer dewatering, possibly because of the low flow rate in the C-1 shaft, the short pumping period, and the distance between the two shafts. Pumping in the C-1 shaft does not have enough time to affect the water level in the Robertson shaft which is pumped at a higher rate (Fig. 9).

Water was simulated to be pumped from the Robertson shaft at different flow rates and depths to reproduce geothermal heat pump system operation (Table 5). The water injection rates in the C-1 shaft were assumed to be equal to the pumping rates. The heat extraction and injection rate were adjusted by increasing the number of buildings to be supplied, aiming to keep the injection temperature above 2 °C. The initial and final temperature of the water pumped and injected from the mine are presented for the simulation

**Fig. 8** Black streamlines indicating heat flux direction and slices showing hydraulic head at the end of 25 years of simulations for a geothermal system operated with a pumping rate of 0.06 m<sup>3</sup> s<sup>-1</sup> and a pump depth of 300 m in the Robertson shaft while water in the Negus shaft is intermittently pumped for dewatering purposes



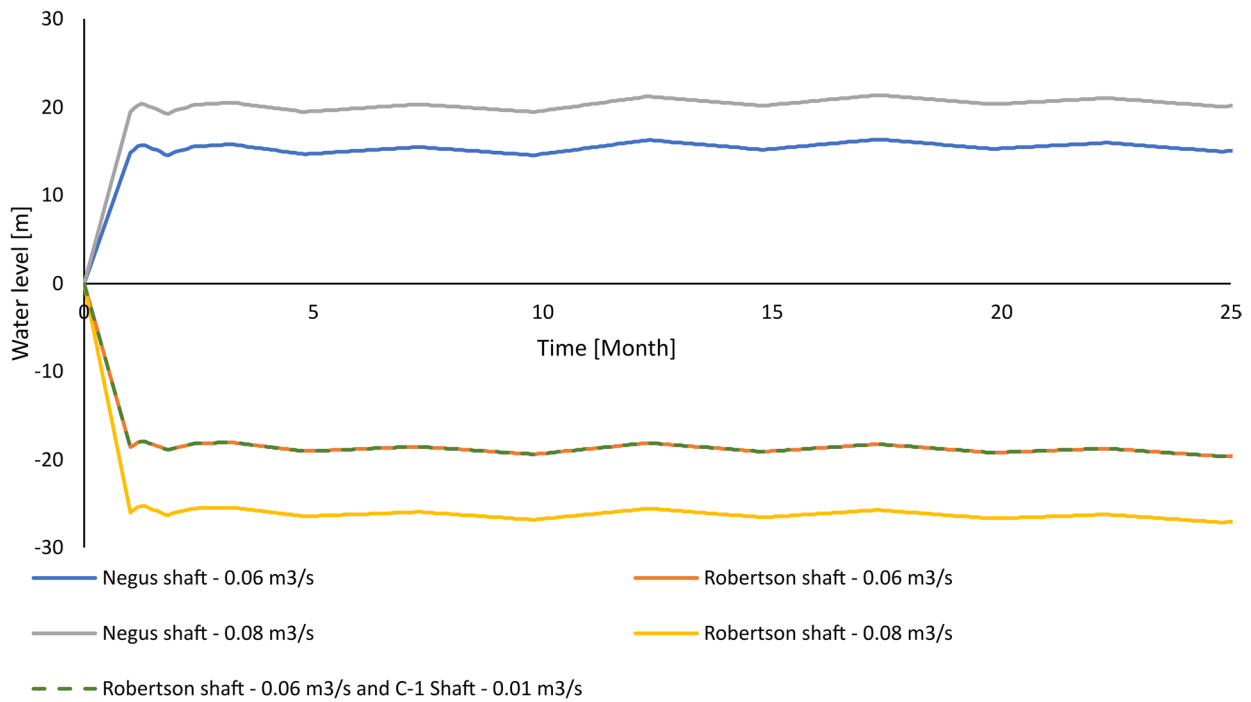


**Fig. 9** Water levels simulated in the Robertson and Negus shafts under the operation of a geothermal heat pump system with and without mine dewatering occurring during summer in the C-1 shaft

without and with solar thermal collectors (Table 6 and 7).

**Table 5** Depth of the pump and flow rate considered for simulations of geothermal heat pump operation with the maximum heat extraction from the mine water during the peak month (January)

Cases	Pump depth m	Flow rate $m^3 s^{-1}$	Maximum thermal power extracted kW
A	300	0.06	562
B	300	0.08	843
C	1	0.06	3,934

The simulated temperatures depend on the depth of the pump, the flow rate, the production temperature, and the heat extracted or injected to the mine water. Temperature differences between the cases with and without solar thermal collectors are illustrated in Figs. 10 and 11.

The production and injection temperature evolve differently for the same number of medium offices (2), with pumping at a flow rate of  $0.06 m^3/s$  for systems with  $8,000 m^2$  of solar thermal collectors and without solar thermal collectors. The production and injection temperature for a system with solar thermal collectors are higher than the case without (Fig. 10), which is due to the additional power generated from the solar thermal collectors during the year. The purpose of these two simulation cases was to show the effect

**Table 6** Production and injection temperature for archetype buildings supplied with a heat pump system having a flow rate of  $0.06 m^3 s^{-1}$  and a pumping depth of 300 m

	Fast food	Retail stand-alone	Outpatient health care	Small hotel	Medium office	Mid-rise apartment
Number of buildings	6	2	2	2	1	5
Production temperature [°C]						
Initial	5.9	5.9	5.9	5.9	5.9	5.9
Final	3.8	3.9	3.9	3.7	3.2	3.9
Injection temperature [°C]						
Initial	4.4	4.7	4.7	4.3	4.9	4.4
Final	2.4	2.0	2.8	2.1	3.0	2.5

**Table 7** Production and injection temperature for archetype buildings supplied with a heat pump system having a flow rate of  $0.06 \text{ m}^3 \text{ s}^{-1}$  and a pumping depth of 300 m including solar thermal collector

	Fast food	Retail stand-alone	Outpatient health care	Small hotel	Medium office	Mid-rise apartment
Number of buildings	7	3	4	3	2	6
Solar area [ $\text{m}^2$ ]	8,000	1,600	104,000	48,000	8,000	8,000
Production temperature [ $^{\circ}\text{C}$ ]						
Initial	5.9	5.9	5.9	5.9	5.9	5.9
Final	3.9	3.9	6.0	4.6	3.8	3.9
Injection temperature [ $^{\circ}\text{C}$ ]						
Initial	4.3	4.7	3.7	4.0	4.1	4.2
Final	2.3	3.0	3.2	2.5	2.0	2.3

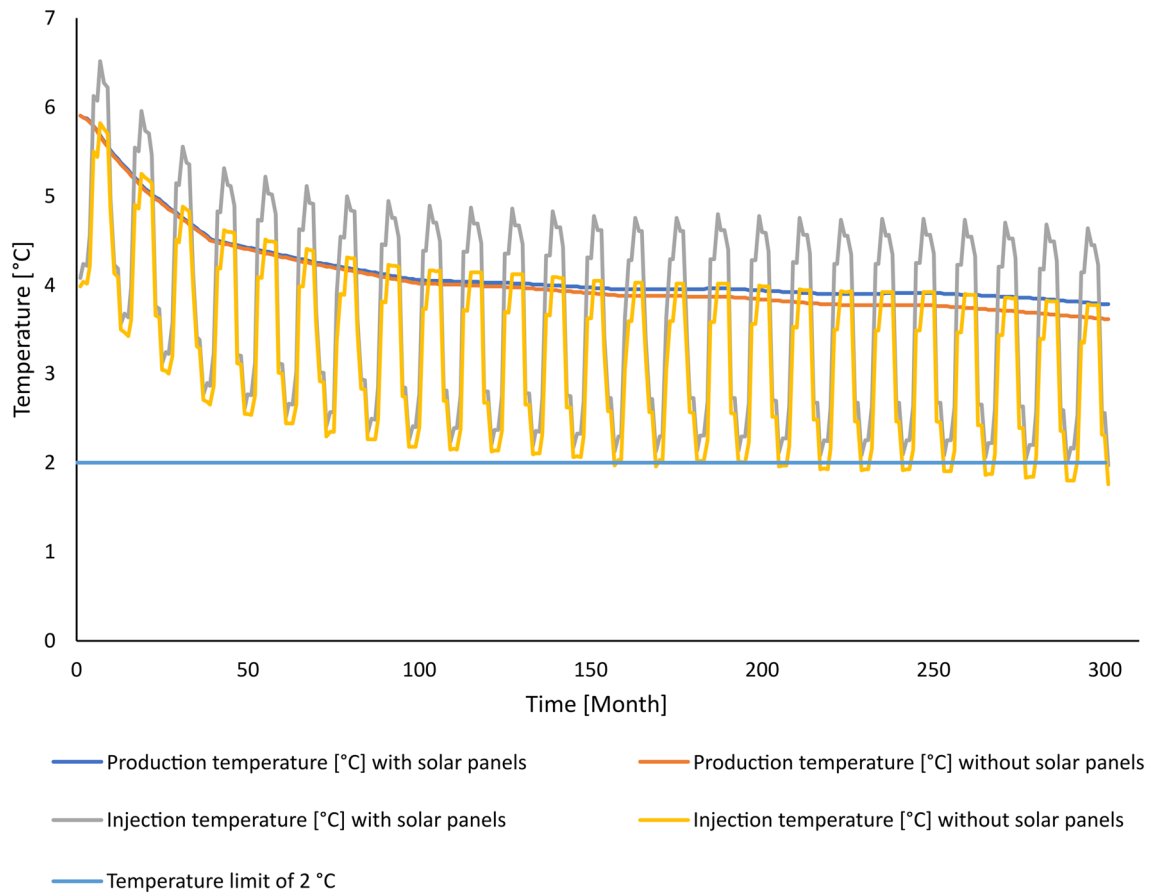


**Fig. 10** Operating water temperature for systems to supply 2 medium offices with and without solar thermal collectors covering  $8 \text{ m}^2$  under a flow rate of  $0.06 \text{ m}^3 \text{ s}^{-1}$  and a pumping depth of 300 m

of solar thermal collectors and to avoid the injected water’s temperature going below  $2 \text{ }^{\circ}\text{C}$ .

The more solar thermal collectors that are installed, the warmer the water injected into the ground will be although solar energy is primarily used for buildings and only injected in the mine water when there is surplus. The results showed

that the needs in solar thermal collectors are based on a building’s needs. Thus, each building requires a different amount of solar thermal collectors. For example, an outpatient health care facility requires more solar thermal collectors than any other building ( $65,000$  solar thermal collectors for  $104,000 \text{ m}^2$ ) and this is the case where there is warmer

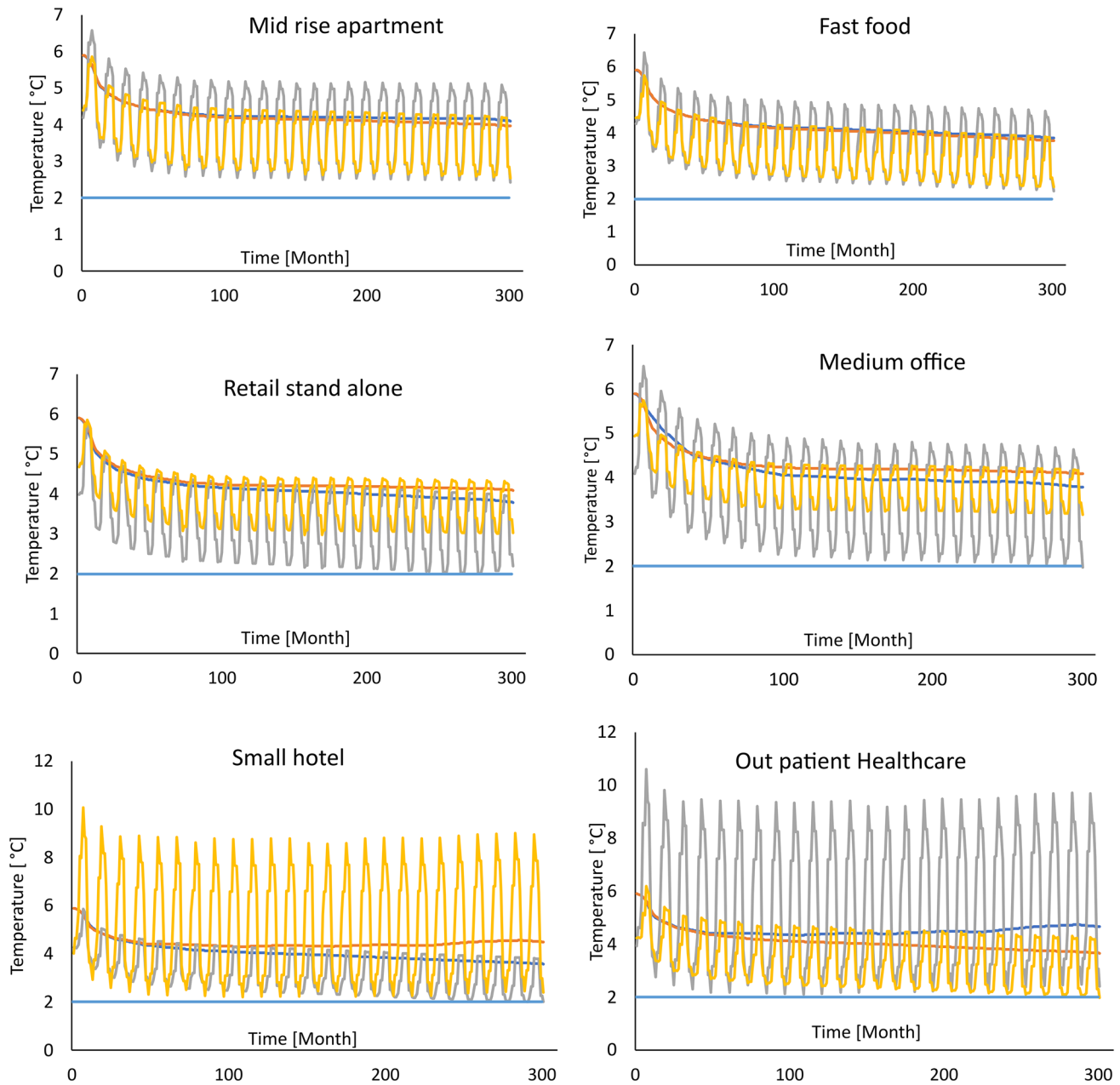


**Fig. 11** Production and injection temperature for all the cases of Table 6 and Table 7. The legend of Fig. 11 is the same as that shown in Fig. 10

water injected because of the excess solar thermal energy. On the other hand, the case of the retail stand-alone does not produce more warm water because the thermal energy is directly used by the buildings (Fig. 11). Injection temperature for the cases of the retail stand-alone and medium office with solar collectors are also lower than cases without solar collectors because of the increased number of buildings that are being heated. Therefore, it does not appear useful to install solar thermal collectors in all cases.

## Number of buildings that can be heated

### Effect of depth and flow rate

Energy extraction and injection from the mine water were simulated according to three cases to determine the maximum number of buildings that can be heated. The same depth (300 m) with two flow rates was initially considered (Case A:  $0.06 \text{ m}^3 \text{ s}^{-1}$ , and Case B:  $0.08 \text{ m}^3 \text{ s}^{-1}$ ; Fig. 12). The third case, Case C considers the same flow rate as Case A ( $0.06 \text{ m}^3 \text{ s}^{-1}$ ), but with a pump at 1 km depth (Fig. 13).

**Fig. 12** Number of buildings that can be heated and cooled with the mine water for pumping at a depth of 300 m and different flow rates of  $0.06 \text{ m}^3 \text{ s}^{-1}$  (case A) and  $0.08 \text{ m}^3 \text{ s}^{-1}$  (case B)

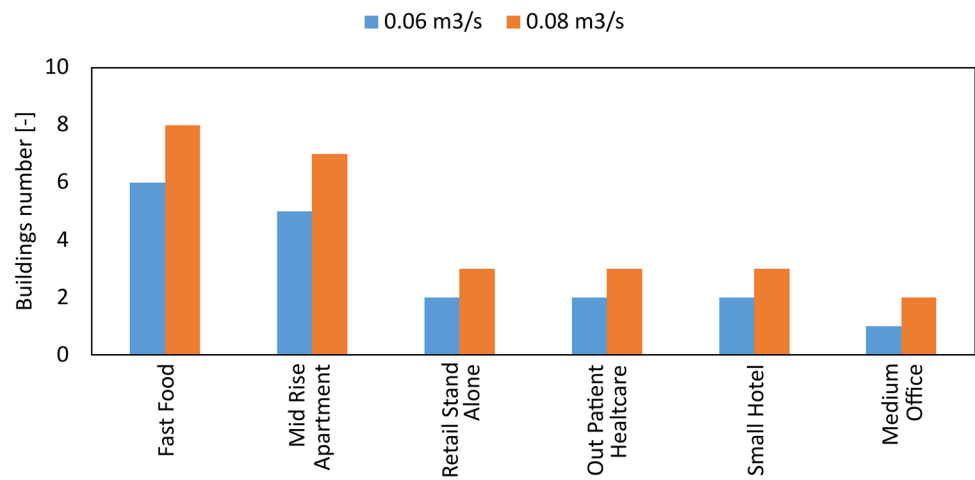
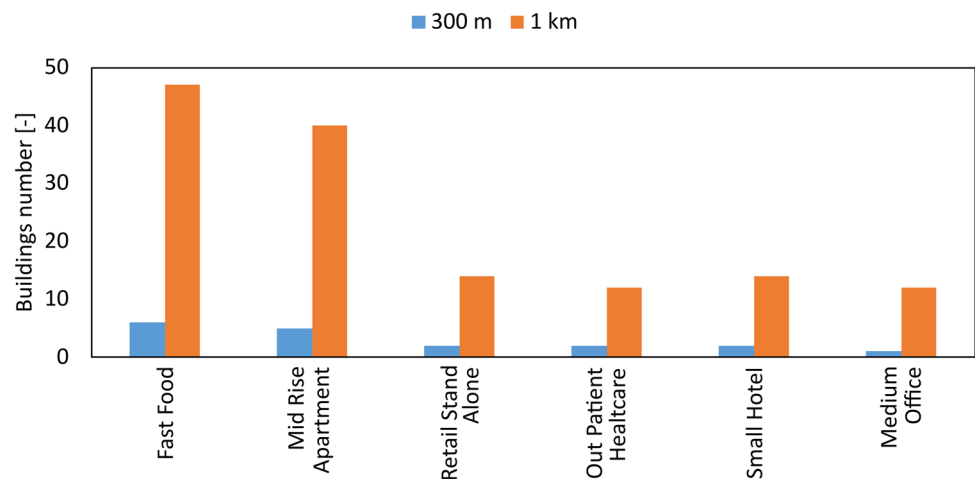


**Fig. 13** Number of buildings that can be heated and cooled with the mine water for the same flow rate of  $0.06 \text{ m}^3 \text{ s}^{-1}$  and different depths of 300 m (case A) and 1 km (case C)



In peak periods, the maximum heat extracted for Case A is 562 kW, for Case B is 843 kW, and for Case C is 3,934 kW. The flow rate of  $0.06 \text{ m}^3 \text{ s}^{-1}$  and a pump depth of 300 m allows at least one building of each category to be adequately heated. Additionally, at this depth, the pump can be placed without technical challenges. Below that depth, there is a possible risk of equipment loss due to the unknown state of the shaft. However, it is possible to heat more buildings by increasing the depth and flow rate. Due to the climatic conditions in Yellowknife, the energy to be delivered for heating buildings exceeds the energy needed for cooling. Table 8 presents the energy that can be supplied to the total number of buildings for each case in Figs. 12 and 13.

### Effect of Adding Solar Thermal Collectors

Instead of increasing the depth of the pump or the flow rate, solar thermal collectors can be used to increase the number of buildings to be heated. When available, surplus energy from solar thermal collectors can be stored in the mine water by the injection of warm water. The number

and area of solar thermal collectors required to add one building in each category were estimated. Simulations were made with a flow rate of  $0.06 \text{ m}^3 \text{ s}^{-1}$  for 25 years, assuming that the pump is placed at 300 m (Table 9). The results were different for each building with different heating loads. The two buildings that required the most solar thermal collectors were the small hotel and the outpatient healthcare, which is due to their high heating demand. Thus, the heat stored in those simulation scenarios was greater than in the other cases. The retail stand-alone was the only case where fewer panels were needed.

### Discussion

The potential of a district geothermal heat pump system at the Con Mine was evaluated with coupled groundwater flow and heat transfer simulations considering building energy needs. The mine workings forming an equivalent porous medium were represented by three-dimensional elements and the mining tunnels and shafts were represented



**Table 8** Heating and cooling load delivered per year to the building for the different study cases

Building	Case A			Case B			Case C		
	Heating [MWh]	Cooling [MWh]	No. of Buildings	Heating [MWh]	Cooling [MWh]	No. of buildings	Heating [MWh]	Cooling [MWh]	No. of buildings
Mid-rise apartment	1,805	115	5	2,166	138	6	14,440	920	40
Fast food	2,304	1.26	6	3,072	1.68	8	18,048	9.87	47
Retail stand-alone	1,028	20	2	1,542	30	3	6,168	120	12
Medium office	953	42	1	1,906	84	2	11,436	504	12
Small hotel	1,978	148	2	2,967	216	3	13,846	1008	14
Outpatient healthcare	2,512	316	2	3,768	474	3	17,584	2212	14

**Table 9** Number of buildings that can be heated with the mine water and solar thermal collector for a flow rate of  $0.06 \text{ m}^3 \text{ s}^{-1}$  and a pump installed at 300 m depth

Building	No. of buildings	No. of solar thermal collectors	Solar thermal collectors area [m <sup>2</sup> ]
Mid-rise apartment	6	5,000	8,000
Fast food	7	5,000	8,000
Retail stand-alone	3	1,000	1,600
Medium office	2	5,000	8,000
Small hotel	3	30,000	48,000
Outpatient healthcare	4	65,000	104,000

with superimposed one-dimensional elements. The numerical model developed for the Con Mine was comparable to the one developed by Boyaud and Therrien (2004), Renz et al. (2009), and Raymond and Therrien (2014) for other mine sites. Renz et al. (2009) developed 2D models of a mine system using a porous media approach. Raymond and Therrien (2014) and Boyaud and Therrien (2004) developed a 3D model where the coupling of elements with different dimensions was considered. Renz et al. (2009) tried both Maning-Strickler and Darcy-Hagen-Poiseuille equations to simulate flow in unidimensional elements embedded into the 2D models. Renz et al. (2009) showed that the flow equation can affect flow velocities and, thus advective heat transfer. Flow in the unidimensional elements of the Con Mine model was computed with Darcy's Law and assumed to be laminar even though local turbulence in mine voids could be expected. This approach allowed us to make simulations with reasonable computational time in a 3D model to evaluate the mine's global thermal response.

Based on pumping and temperature measurement achieved at the C-1 shaft, the model was manually calibrated to reproduce the trend in hydraulic head and temperature from the dewatering activities. The global hydraulic and thermal response of the flooded mine system was reproduced although some discrepancy remained between the simulated and measured hydraulic head and temperature. Difficulty encountered with calibration can be due to the complex mine geometry that is simplified in the numerical model. However, the permeability assigned to the porous medium adequately reproduced the hydraulic response of the underground mine such that predictive simulations could be undertaken. Indeed, the permeability of the host rock is the parameter that dominantly influences the water level in the shaft. This finding agrees with Raymond and Therrien (2014), who showed that hydraulic conductivity was the main parameter influencing the water level in the mine system. The temperature measured at the mine site was more challenging to replicate. The dewatering outlet zone is where water is exposed to atmospheric conditions and is a mix of

water coming from various depths, which can create temperature fluctuations that cannot be replicated exactly. The temperature was not influenced by the permeability but by the porosity. However, the influence is weak.

Simulations achieved for the Con Mine indicate that the site geothermal potential is a function of the flow rate and the pumping depth expected for the operation of the geothermal system and affecting the production temperature. Simultaneous pumping made seasonally to dewater the mine had a negligible effect on the operation of the geothermal system since the dewatering flow rate was less important than the operating geothermal flow rate, which is continuous rather than intermittent (Fig. 9). The results showed that increasing the flow rate and the depth of the pump allowed more energy production (Tables 6 and 7), as found in Raymond and Therrien (2014). Moreover, the addition of solar thermal collectors and allowing surplus heat to be stored underground can help increase the production temperature and thus the thermal energy output. Indeed, the results forecast that the injection temperature was higher in most cases with solar thermal collectors.

The comparison of the geothermal potential from the Con Mine to other mines is possible, but in a limited manner because the potential of other sites was evaluated for different periods and with different purposes. Moreover, the potential calculated in this work was based on heating demand for buildings adapted to Yellowknife weather conditions. Renz et al. (2009) estimated an available energy of 43.8 GWh per year at the Stassfurt potassium mine site for a volume of  $2.18 \times 10^6 \text{ m}^3$  of water and a flow rate of  $3.5 \times 10^{-3} \text{ m}^3 \text{ s}^{-1}$ . At the Gaspé mine with the maximum flow rate of  $0.063 \text{ m}^3 \text{ s}^{-1}$ , Raymond and Therrien (2014) evaluated the available energy to 5 MWh per year. In Pennsylvania, West Virginia, and Ohio, a single coal seam contains  $5.1 \times 10^9 \text{ m}^3$  of water. The growing volume of water discharging from this single coal seam totals  $6.3 \text{ m}^3 \text{ s}^{-1}$ , which could theoretically produce 437 GWh annually (Watzlaf and Ackman 2006). Those previous studies show a large range of energy that can be produced reflecting each mine's characteristics. In comparison to these other mines, the annual geothermal energy delivered to buildings using the Con Mine system was simulated to range between 953 to 18,048 MWh, depending on the flow rate and the depth of pumping in the mining shaft.

Our simulations further show that adding solar thermal collectors to a potential district heating system and storing the surplus energy in the mine may not add a significant advantage. Adding solar thermal collectors did increase the temperature of water stored in most cases and, therefore, the production and injection temperature, but the number of solar thermal collectors was important. Indeed, the heating potential can be more easily increased with an increased depth of pumping or flow rate. However, in the Con Mine

case, access to the mine water at greater depths may be difficult due to the unknown state of the shaft below 300 m. Where it is not possible to install a pump deeper, solar thermal collectors can provide an alternative to increase the system capacity.

This study allowed us to evaluate the number of buildings that could be heated using a geothermal heat pump system feed by the mine water for a period of 25 years. The heating and cooling demands for the different buildings was determined considering the climate of Yellowknife. The number of buildings thus varies with the heat demand, such that it can be possible to supply more individual fast food restaurants (6) than small hotels (2) at a flow rate of  $0.06 \text{ m}^3 \text{ s}^{-1}$  and a pumping depth of 300 m. Moreover, the number of buildings that can be supplied should be seen as a minimum because simulations were made assuming that individual buildings connect in series to a hypothetical district heating system that was not optimized.

## Conclusions

This work showed that the Con Mine holds enough thermal energy to sustainably heat and cool various buildings in Yellowknife with a heat pump for over 25 years. These buildings can be heated with the thermal energy delivered from a geothermal heat pump system alone or a combination of geothermal heat pump systems coupled with solar thermal collectors and underground energy storage. If only a geothermal heat pump system is used, simulations indicated that the heat delivered to the buildings depends on two main factors: the depth of pumping and the flow rate supplied to the heat pump. The energy delivered to the buildings can annually reach 2,512 MWh at a pump depth of 300 m for a flow rate of  $0.06 \text{ m}^3 \text{ s}^{-1}$ , while it increases to 3,768 MWh if the flow rate is  $0.08 \text{ m}^3 \text{ s}^{-1}$ . The thermal power extracted from the mine water during peak conditions is 562 kW and 843 kW in both cases. This would allow heating of either 5 to 6 mid-rise apartments, 6 to 8 fast food restaurants, 2 to 3 retail stand-alone buildings, 1 to 2 medium office buildings, 2 to 3 small hotels, or 2 to 3 outpatient healthcare facilities in the climate of Yellowknife. Installing the pump at a greater depth would increase the thermal energy annually delivered to buildings, with up to 18,048 MWh for a pump located at 1 km depth, offering a heating capacity of 3.9 MW in peak conditions. Previous assessment of the geothermal potential of the Con Mine indicated a heat extraction potential of 0.3 MW when considering the volume of water that can be cooled down (Ghomshei 2007), 0.4 MW when evaluating the Earth's natural heat flow only (Ferket et al. 2012), and 2 MW when using a thermal power budget calculation that considers the thermal mass of the mine water and the surrounding bedrock (Ngoyo Mandemvo 2023). The numerical

models developed in this study showed a higher geothermal potential, which is now better estimated because convective heat transfer was considered in the simulations. Developing such a numerical model was challenging but implementing a thermal power budget approach to estimate the geothermal potential of mine site is easier (Ngoyo Mandemvo 2023) and can be done at an earlier stage of resource assessment to justify if further numerical model development is required to fully assess a mine site's geothermal potential.

The next step to develop geothermal resources of the Con Mine is to design a district heating system to exploit the mine water. Moreover, the district system configuration could be optimized to recover thermal energy when possible and supply more buildings. Then, a small-scale exploitation could be initiated to validate the geothermal district heating concept and assess its feasibility.

**Supplementary Information** The online version contains supplementary material available at <https://doi.org/10.1007/s10230-024-00976-4>.

**Acknowledgements** The support of the Northwest Territories Geological Survey, the Geological Survey of Canada, Newmont Mining Corp, and the funding of the Northern Geothermal Potential Research Chair by the Institut nordique du Québec is acknowledged.

## References

- Banks D, Skarphagen H, Wiltshire R, Jessop C (2004) Heat pumps as a tool for energy recovery from mining wastes. In: Gieré R, Stille P (eds), *Energy, waste and the environment: a geochemical perspective*, vol 236, Geological Society Publishing House, Bath, pp 499–513. DOI:<https://doi.org/10.1144/GSL.SP.2004.236.01.27>
- Bao T, Liu Z (2019) Geothermal energy from flooded mines: modeling of transient energy recovery with thermohaline stratification. *Energy Con Manag* 199. <https://doi.org/10.1016/j.enconman.2019.111956>
- Bhowmik H, Amin R (2017) Efficiency improvement of flat plate solar collector using reflector. *Energy Rep* 3:119–123. <https://doi.org/10.1016/j.egy.2017.08.002>
- Boyaud C, Therrien R (2004) Numerical modeling of mine water rebound in Saizerais, northeastern France. In: Miller CT, Farthing MW, Gray WG, Pinder GF (eds) *Proc, 15<sup>th</sup> International Conf on Computational Methods in Water Resources*, vol 2. *Developments in Water Science* 55. Elsevier, Chapel Hill, North Carolina, pp 977–989
- Cairns S, Hauser R (1995) *Yellorex south drilling*. Internal Report, Miramar Con Mine Ltd, Yellowknife
- Caneta research (1997) *Municipal building, Park Hills, Missouri – technical report*. Internal Report, Geothermal Heat Pump Consortium, Mississauga
- Comsol AB (2017) *Heat Transfer Module User's Guide*. User's Manual, Version 5.3a, Comsol, Stockholm
- Energy plus (2021) *All Regions—North and Central America (WMO Region 4)—Canada—Northwest Territories (9.4.0)*. Computer software. <https://energyplus.net/>. Accessed 02/09/2020
- Energysage (2021) How much energy does a solar panel produce? Solar panel output explained. *Energysage*, smarter energy decisions. <https://news.energysage.com/what-is-the-power-output-of-a-solar-panel/#comments>. Accessed 23/10/2021.
- Environment and Climate Change Canada (2021) *Engineering Climate Datasets*. Environment and Climate Change Canada. [https://climate.weather.gc.ca/prods\\_servs/engineering\\_e.html](https://climate.weather.gc.ca/prods_servs/engineering_e.html). Accessed 05/10/2021
- Ferket H, Ben L, Tongeren P (2011) Transforming flooded coal mines to large-scale geothermal and heat storage reservoirs: What can we expect? 11th International Mine Water Association Congress – Mine Water – Managing the Challenges, Aachen
- Ferket H, Laenen B, Harcouët-Menou V, Lagrou D, Van Tongeren P (2012) Evaluation of Con Mine energy resource. Presentation, VITO, Yellowknife
- Ghomshei MM (2007) *Geothermal energy from Con Mine for Heating the City of Yellowknife, NWT: a concept study*. Internal Report, City of Yellowknife, University of British Columbia, Vancouver
- Ghoreishi Madiseh SA, Ghomshei MM, Hassani FP, Abbasy F (2012) Sustainable heat extraction from abandoned mine tunnels: A numerical model. *Journal Renew Sustain Energy* 4(3):033102. <https://doi.org/10.1063/1.4712055>
- Gilbert J (2021a) *Glenalmond street project*. John Gilbert Architects, Glasgow. [http://www.johngilbert.co.uk/?portfolio\\_page=glenalmond-street](http://www.johngilbert.co.uk/?portfolio_page=glenalmond-street). Accessed 25/10/2021
- Gilbert J (2021b) *Lumphinnans sustainable housing project*. John Gilbert Architects, Glasgow. [http://www.johngilbert.co.uk/?portfolio\\_page=lumphinnans](http://www.johngilbert.co.uk/?portfolio_page=lumphinnans). Accessed 25/10/2021.
- Grasby S, Allen D, Bell S, Chen Z, Ferguson G, Jessop AM, Kelman M, Ko M, Majorowicz J, Moore M, Raymond J, Therrien R (2012) *Geothermal Energy Resource Potential of Canada*. Geological Survey of Canada, Open File 6914, Calgary
- Hall A, Scott JA, Shang H (2011) Geothermal energy recovery from underground mines. *Renew Sust Energy Rev* 15(2):916–924. <https://doi.org/10.1016/j.rser.2010.11.007>
- Jardón S, Ordóñez A, Álvarez R, Cienfuegos P, Loredó J (2013) Mine water for energy and water supply in the central coal basin of Asturias (Spain). *Mine Water Environ* 32(2):139–151. <https://doi.org/10.1007/s10230-013-0224-x>
- Jessop AM, Ghomshei MM, Drury MJ (1991) Geothermal energy in Canada. *Geothermics* 20(5):369–385. [https://doi.org/10.1016/0375-6505\(91\)90027-S](https://doi.org/10.1016/0375-6505(91)90027-S)
- Jessop AM (2005) *The Canadian geothermal data compilation*. Geological Survey of Canada, Open File 4887. <https://geoscan.nrcan.gc.ca/starweb/geoscan/servlet.starweb?path=geoscan/fulle.web&search1=R=220364>
- Kranz K, Dillenardt J (2010) Mine water utilization for geothermal purposes in Freiberg, Germany: determination of hydrogeological and thermophysical rock parameters. *Mine Water Environ* 29(1):68–76. <https://doi.org/10.1007/s10230-009-0094-4>
- Krawczyk DA, Żukowski M, Rodero A (2020) Efficiency of a solar collector system for the public building depending on its location. *Environ Sci Pollut Res* 27(1):101–110. <https://doi.org/10.1007/s11356-019-05077-2>
- Loredó C, Roqueñí N, Ordóñez MA (2016) Modelling flow and heat transfer in flooded mines for geothermal energy use: a review. *Int J Coal Geol* 164:115–122. <https://doi.org/10.1016/j.coal.2016.04.013>
- Lund JW, Toth AN (2021) Direct utilization of geothermal energy 2020 worldwide review. *Geothermics* 90:101915. <https://doi.org/10.1016/j.geothermics.2020.101915>
- Lund, JW (2018) *Geothermal Energy*. *Encyclopedia Britannica*. <https://www.britannica.com/science/geothermal-energy>. Accessed 18/05/2022.
- Małolepszy Z (2003) Low-temperature, man-made geothermal reservoirs in abandoned workings of underground mines. In: *Proceedings of, 28th Workshop on Geothermal Reservoir Engineering*, Stanford Univ, Stanford, pp. 259–265

- Matthes R, Schreyer J (2007) Remediation of the Old Wismut shaft 302 in Marienberg and installation of a technical plant for geothermic mine water use (Ore Mountains, Germany). Proc, International Mine Water Assoc Symp – Water in Mining Environments, Cagliari, pp 227–231
- Miramar Con Mine Ltd (2007). Final closure and reclamation plan. Internal Report, Miramar Con Mine Ltd, Yellowknife. <https://bit.ly/3air9IE>. Accessed 03/04/2020
- Muffler P, Cataldi R (1978) Methods for regional assessment of geothermal resources. *Geothermics* 7(2):53–89. [https://doi.org/10.1016/0375-6505\(78\)90002-0](https://doi.org/10.1016/0375-6505(78)90002-0)
- Ngoyo Mandemvo DD, Comeau F-A, Raymond J, Grasby SE, Terlaky V (2023) Geothermal potential of closed underground mines: resource assessment study of the Con Mine, Northwest Territories, Canada. *Nat Resour Res* 32:1579–1593. <https://doi.org/10.1007/s11053-023-10214-3>
- Ngoyo Mandemvo DD (2022) Potentiel géothermique des mines inondées: étude de la mine Con. Master's Thesis. Institut National de la Recherche Scientifique, Quebec City
- Northwest Territories Geological Survey (2021) Map of the geological provinces of the Northwest Territories. Northwest Territories Geological Survey, Yellowknife. <https://webapps.nwtgeoscience.ca/Html5Viewer/index.html?viewer=NTGSwebGIS2.NTGSwebGIS>. Accessed 12/09/2021
- Ordóñez A, Jardón S, Álvarez R, Andrés C, Pendás F (2012) Hydrogeological definition and applicability of abandoned coal mines as water reservoirs. *J Environ Monit* 14(8):2127–2136. <https://doi.org/10.1039/C2EM11036A>
- Ouzzane M, Eslami-Nejad P, Badache M, Aidoun Z (2015) New correlations for the prediction of the undisturbed ground temperature. *Geothermics* 53:379–384. <https://doi.org/10.1016/j.geothermics.2014.08.001>
- Padgham WA (1980) An Archean ignimbrite at Yellowknife and its relationship to the Kam Formation basalts. *Precambrian Res* 12(1):99–113. [https://doi.org/10.1016/0301-9268\(80\)90025-X](https://doi.org/10.1016/0301-9268(80)90025-X)
- Raymond J, Therrien R (2014) Optimizing the design of a geothermal district heating and cooling system located at a flooded mine in Canada. *Hydrogeol J* 22(1):217–231. <https://doi.org/10.1007/s10040-013-1063-3>
- Renz A, Rühaak W, Schätzl P, Diersch H-JG (2009) Numerical modeling of geothermal use of mine water: challenges and examples. *Mine Water Environ* 28(1):2–14. <https://doi.org/10.1007/s10230-008-0063-3>
- Roy D, Chakraborty T, Basu D, Bhattacharjee B (2020) Feasibility and performance of ground source heat pump systems for commercial applications in tropical and subtropical climates. *Renew Energ* 152:467–483. <https://doi.org/10.1016/j.renene.2020.01.058>
- Sarbu I, Sebarchievici C (2017) Solar Collectors. Ch 3 in: Sarbu I, Sebarchievici C (Eds), *Solar Heating and Cooling Systems*, Academic Press. <https://doi.org/10.1016/B978-0-12-811662-3.00003-7>
- Sunmin K (2021) Real-time flood forecasting with weather radar and distributed hydrological model. In: Samui P, Bonakdari H, Deo R (Eds), *Water Engineering Modeling and Mathematic Tools*, Elsevier. <https://doi.org/10.1016/B978-0-12-820644-7.00024-4>
- Toth AN (2007) A prospect geothermal potential of an abandoned copper mine. Proc, 32<sup>nd</sup> Workshop on Geothermal Reservoir Engineering, Stanford Univ, Stanford, pp 1–3
- Watzlaf GR, Ackman TE (2006) Underground mine water for heating and cooling using geothermal heat pump systems. *Mine Water Environ* 25(1):1–14. <https://doi.org/10.1007/s10230-006-0103-9>
- Wieber G, Pohl S (2008) Mine water: a source of geothermal energy—examples from the Rhenish Massif. Proc, 10<sup>th</sup> International Mine Water Assoc Congress, Karlovy Vary, pp 113–116
- Wolkersdorfer C (2006) Water Management at Abandoned Flooded Underground Mines: Fundamentals, Tracer Test, Modelling, Water Treatment. Springer, Heidelberg. <https://www.wolkersdorfer.info/publication/pdf/MineAbandonment.pdf>
- Yellowlite (2021) The Advantages of Different Types of Premium Solar Panels. Yellowlite Harvesting Clean Energy. <https://www.yellowlite.com/blog/post/the-advantages-of-different-types-of-premium-solar-panels/>. Accessed 11/11/2021

Springer Nature or its licensor (e.g. a society or other partner) holds exclusive rights to this article under a publishing agreement with the author(s) or other rightsholder(s); author self-archiving of the accepted manuscript version of this article is solely governed by the terms of such publishing agreement and applicable law.